Journal of Alloys and Compounds 509 (2011) 499–502

Contents lists available at ScienceDirect

Journal of Alloys and Compounds

journal homepage: www.elsevier.com/locate/jallcom

Structure and thermal behavior of multicomponent $Fe_{68-x}Ni_xZr_{15}Nb_5B_{12}$ (x = 5, 10, 15, 20) alloys

Y.M. Sun*

College of Physics, Jilin Normal University, No. 1301, Haifeng Street, Tiexi Area, Siping, Jilin 136000, PR China

ARTICLE INFO

Article history:
Received 28 March 2010
Received in revised form
14 September 2010
Accepted 17 September 2010
Available online 24 September 2010

Keywords:
Mechanical alloying
Thermal analysis

ABSTRACT

Multicomponent $Fe_{68-x}Ni_xZr_{15}Nb_5B_{12}$ (x = 5, 10, 15, 20) alloy powders milled for 60 h were prepared by mechanical alloying (MA). The structure and crystallization behavior were investigated by X-ray diffraction (XRD), scanning electron microscopy (SEM) and differential thermal analysis (DTA). Ni enhances the amorphisation of alloy powders. Particle size increases with increasing Ni content. Both onset crystallization temperature T_x and the first crystallization peak temperature T_p of the four alloys shift to a higher temperature with increasing heating rate while melting temperature (T_m) is just the opposite. $Fe_{68-x}Ni_xZr_{15}Nb_5B_{12}$ (x = 5, 10, 15, 20) alloys all have a large supercooled liquid region ΔT_x. The supercooled liquid region ΔT_x increases and the crystallization activation energy E decreases with increasing Ni content.

1. Introduction

Mechanical alloying (MA) is a solid-state powder processing technique involving repeated welding, fracturing, and rewelding of powder particles in a high-energy ball mill [1]. MA is employed to synthesize a variety of stable and metastable materials, including supersaturated solid solutions, intermetallics, amorphous alloys and so on [2].

Extensive studies on Fe-based alloys prepared by MA have been carried out, and their structure [3–6], magnetic property [5–7], and crystallization behavior [8,9] have been investigated in detail. The study of the crystallization behavior is very important in understanding the thermal stability of amorphous phase [8]. The glass forming ability (GFA) of alloys can be evaluated by a temperature span of the supercooled liquid region ΔT_x (difference between the glass transition temperature T_g and the onset crystallization temperature T_x). The wider is the ΔT_x, the greater is the GFA [10].

A large number of multicomponent alloy systems have been identified with high GFA [11]. The effect of multicomponent is probably due to the "confusion principle": the more elements involved, the lower the chance that the alloy can select viable crystal structures, and the greater the chance of glass formation [12]. The large supercooled liquid regions of Fe-based alloys are observed in $Fe_{56}Co_7W_2Mo_5Zr_{10}B_{20}$ alloy (92 K) prepared by copper mould casting [13] and $(Fe_{50}Co_{50})_{62}Nb_8B_{30}$ alloy (102 K) prepared by melt spinning [14]. In this work, multicomponent $Fe_{68-x}Ni_xZr_{15}Nb_5B_{12}$ (x = 5, 10, 15, 20) alloys prepared by MA with large supercooled liquid regions ΔT_x were successfully produced. The structure and crystallization behavior of alloy powders were studied.

2. Experimental details

Samples with nominal composition of $Fe_{68-x}Ni_xZr_{15}Nb_5B_{12}$ (x = 5, 10, 15, 20) were prepared by MA. Fe, Ni, Zr, Nb and B powders with a purity above 99% were sealed in a cylindrical stainless steel vial (100 ml in volume) together with 60 stainless steel balls (8 mm in diameter) and milled under an argon atmosphere. The milling procedure was carried out at room temperature by mounting the vial in a GN-2 planetary ball mill. The ball-to-powder weight ratio was 30:1. The alloy powders milled for 60 h were collected.

Structural characterization of samples was examined by X-ray diffraction (XRD, D/max 2500/PC, Cu-Kα, λ = 1.5406 Å) and scanning electron microscopy (SEM, S-570). The crystallization analysis was investigated by differential thermal analysis (DTA, PE TG/DTA-6300) at different heating rates (10, 20 and 30 K/min). Detailed thermal analysis of samples revealed a spectrum of values for glass transition temperature T_g, onset crystallization temperature T_x, the first crystallization peak temperature T_p and melting temperature T_m.

3. Results and discussion

XRD patterns of $Fe_{68-x}Ni_xZr_{15}Nb_5B_{12}$ (x = 5, 10, 15, 20) alloy powders milled for 60 h are shown in Fig. 1. Broad diffraction halos are the main features in the XRD, indicating that the alloy powders milled for 60 h are predominant amorphous. The peak intensity decreases with increasing Ni content. Ni enhances the amorphisation of alloy powders.

SEM images of $Fe_{68-x}Ni_xZr_{15}Nb_5B_{12}$ (x = 5, 10, 15, 20) alloy powders milled for 60 h are shown in Fig. 2. Along with the increase of x, particle size increases. The variation in powder particle size may be ascribed to the welding between elements. Ni is more

* Tel.: +86 434 3294593; fax: +86 434 3294566.
E-mail address: sunyaming2007@126.com.

0925-8388/$ – see front matter © 2010 Elsevier B.V. All rights reserved.
doi:10.1016/j.jallcom.2010.09.079

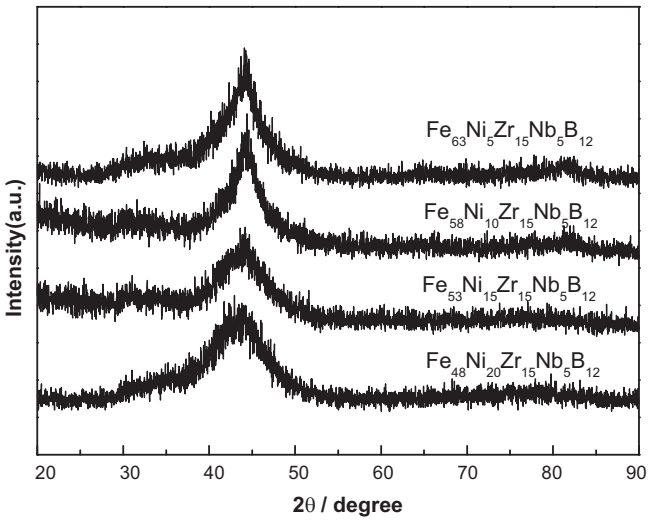

Fig. 1. XRD patterns of $Fe_{68-x}Ni_xZr_{15}Nb_5B_{12}$ (x = 5, 10, 15, 20) alloy powders milled for 60 h.

ductile than Fe, and Ni substitution for Fe enhances the welding of powder particles. Liu et al. [15] considered that the driving force for welding can be the heat of mixing between elements. The heats of mixing (kJ/mol) [16] between Fe(Ni) and other elements are shown in Table 1. The heat of mixing of alloy powders

Table 1
The heats of mixing (kJ/mol) between Fe(Ni) and other elements.

	Zr	Nb	B
Fe	−25	−16	−26
Ni	−49	−30	−24

increases on the whole with increasing Ni content, so particle size increases.

Fig. 3 shows the DTA traces of $Fe_{63}Ni_5Zr_{15}Nb_5B_{12}$ alloy at different heating rates. Both T_x and T_p shift to a higher temperature with increasing heating rate. However, T_m shifts to a lower temperature. The variations of T_x, T_p and T_m of $Fe_{68-x}Ni_xZr_{15}Nb_5B_{12}$ (x = 10, 15, 20) alloys with increasing heating rate are the same as $Fe_{63}Ni_5Zr_{15}Nb_5B_{12}$ alloy.

Fig. 4 shows the DTA traces of $Fe_{68-x}Ni_xZr_{15}Nb_5B_{12}$ (x = 5, 10, 15, 20) alloys at a heating rate of 20 K/min. T_m remains almost constant (1253 K) with increasing Ni content. T_g, T_x and ΔT_x of $Fe_{68-x}Ni_xZr_{15}Nb_5B_{12}$ (x = 5, 10, 15, 20) alloys as a function of Ni content are shown in Fig. 5. ΔT_x increases with increasing Ni content and these alloys all have a large supercooled liquid region ΔT_x. The increase of Ni content enhances the GFA, which corresponds to the results of XRD. The large GFA is believed to satisfy the three empirical rules, i.e. multicomponent systems consisting of more than three constituent elements, significant atomic size ratios above 12%, and negative heats of mixing among the main constituent elements [17]. There is significant difference in atomic size ratios above 12% among the main constituent ele-

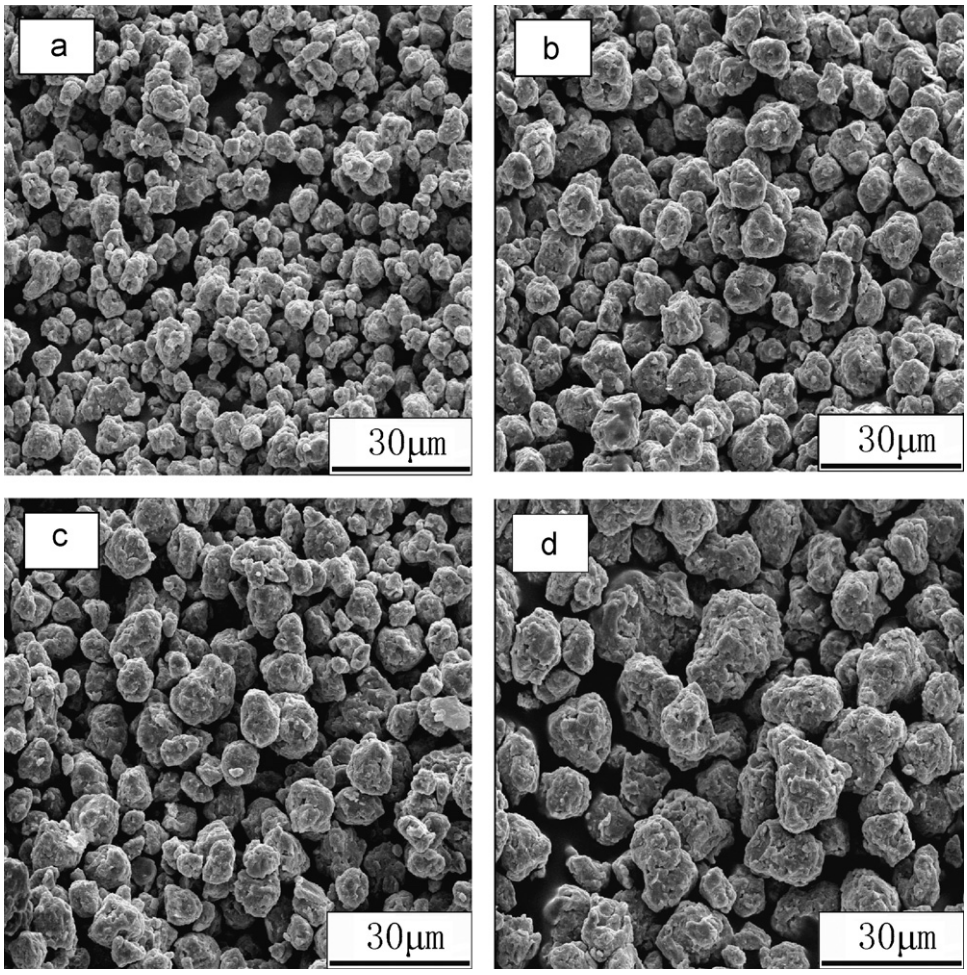

Fig. 2. SEM images of $Fe_{68-x}Ni_xZr_{15}Nb_5B_{12}$ (x = 5, 10, 15, 20) alloy powders milled for 60 h: (a) $Fe_{63}Ni_5Zr_{15}Nb_5B_{12}$; (b) $Fe_{58}Ni_{10}Zr_{15}Nb_5B_{12}$; (c) $Fe_{53}Ni_{15}Zr_{15}Nb_5B_{12}$; (d) $Fe_{48}Ni_{20}Zr_{15}Nb_5B_{12}$.

Table 2
T_p (K) of $Fe_{68-x}Ni_xZr_{15}Nb_5B_{12}$ (x = 5, 10, 15, 20) alloys obtained at different heating rates.

ν (K/min)	$Fe_{63}Ni_5Zr_{15}Nb_5B_{12}$	$Fe_{58}Ni_{10}Zr_{15}Nb_5B_{12}$	$Fe_{53}Ni_{15}Zr_{15}Nb_5B_{12}$	$Fe_{48}Ni_{20}Zr_{15}Nb_5B_{12}$
10	890.1	914.1	901.0	895.8
20	902.8	915.8	919.1	923.2
30	908.1	929.4	922.0	925.3

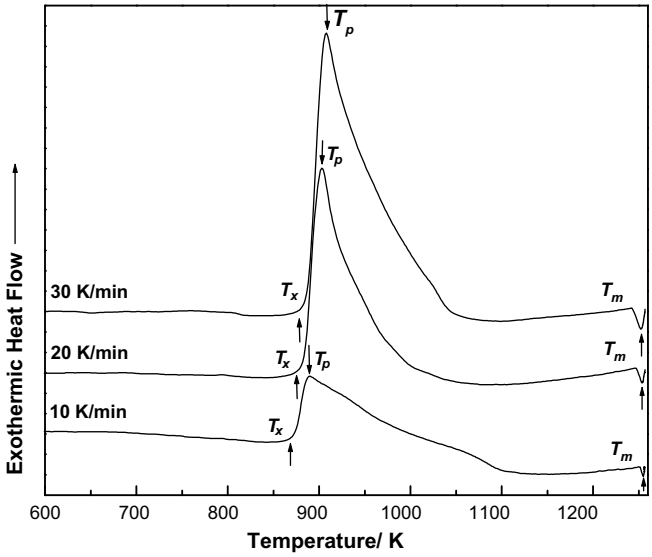

Fig. 3. DTA traces of $Fe_{63}Ni_5Zr_{15}Nb_5B_{12}$ alloy at different heating rates.

ments of FeNiZrNbB alloy system and the sequence of atomic size is Zr > Nb ≫ Fe > Ni ≫ B. The alloy system has high negative heats of mixing among the elements (Table 1).

The crystallization activation energy E is calculated using Kissinger equation [18] by plotting $\ln(\nu/T^2)$ versus $1/T$ (a straight line with the slope of E/R can be obtained), where R is the gas constant, ν is the heating rate (K/min) and T is a specific absolute temperature such as T_g, T_x or T_p. Table 2 shows the T_p of $Fe_{68-x}Ni_xZr_{15}Nb_5B_{12}$ (x = 5, 10, 15, 20) alloys obtained at different heating rates. The Kissinger plots for T_p are shown in Fig. 6.

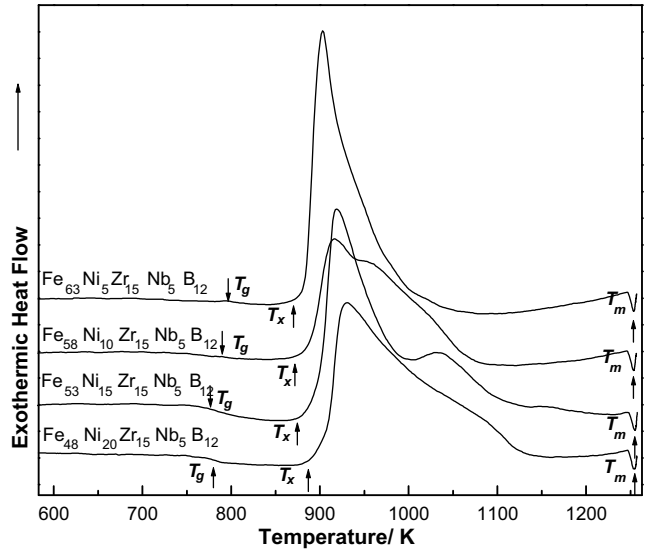

Fig. 4. DTA traces of $Fe_{68-x}Ni_xZr_{15}Nb_5B_{12}$ (x = 5, 10, 15, 20) alloys at a heating rate of 20 K/min.

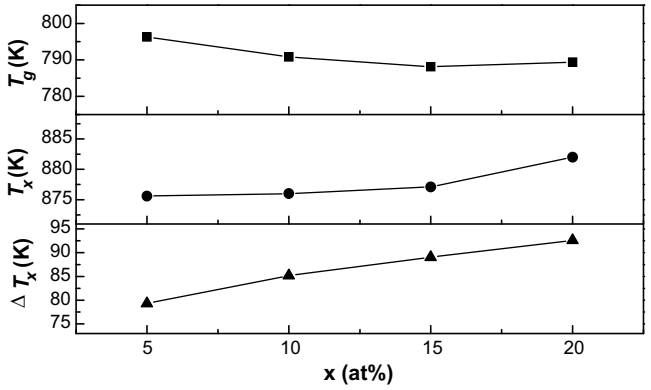

Fig. 5. T_g, T_x and ΔT_x of $Fe_{68-x}Ni_xZr_{15}Nb_5B_{12}$ (x = 5, 10, 15, 20) alloys as a function of Ni content.

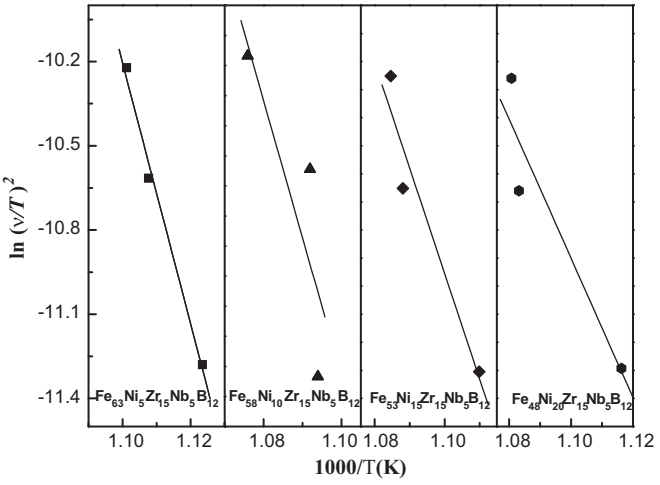

Fig. 6. Kissinger plots of $Fe_{68-x}Ni_xZr_{15}Nb_5B_{12}$ (x = 5, 10, 15, 20) alloys.

The crystallization activation energies E of $Fe_{68-x}Ni_xZr_{15}Nb_5B_{12}$ (x = 5, 10, 15, 20) alloys are 386.3, 378.8, 311.4 and 205.9 kJ/mol, respectively. E decreases with increasing Ni content. That is to say, the increase of Ni content weakens the thermal stability.

4. Conclusions

(1) $Fe_{68-x}Ni_xZr_{15}Nb_5B_{12}$ (x = 5, 10, 15, 20) alloy powders milled for 60 h are predominantly amorphous. Ni enhances the amorphisation of alloy powders. Particle size increases with increasing Ni content, which is due to the increase of the heat of mixing.
(2) Both onset crystallization temperature T_x and the first crystallization peak temperature T_p shift to a higher temperature with increasing heating rate while melting temperature (T_m) is just the opposite.
(3) $Fe_{68-x}Ni_xZr_{15}Nb_5B_{12}$ (x = 5, 10, 15, 20) alloys all have a large supercooled liquid region ΔT_x and ΔT_x increases. The increase of Ni content enhances the GFA.

(4) The crystallization activation energy E of $Fe_{68-x}Ni_xZr_{15}Nb_5B_{12}$ (x = 5, 10, 15, 20) alloys decreases with increasing Ni content. The increase of Ni content weakens the thermal stability.

Acknowledgement

This work was funded by Science and Technology Development Project of Jilin Province (No. 20082112).

References

[1] C. Suryanarayana, Prog. Mater. Sci. 46 (2001) 1–184.
[2] A. Tonejc, Acta Chim. Slov. 49 (2002) 1–28.
[3] J.S. Blázquez, J.J. Ipus, M. Millán, V. Franco, A. Conde, D. Oleszak, T. Kulik, J. Alloys Compd. 469 (2009) 169–178.
[4] J.J. Suñol, J.M. Güell, J. Bonastre, S. Alleg, J. Alloys Compd. 483 (2009) 604–607.
[5] S. Alleg, M. Ibrir, N.E. Fenineche, S. Azzaza, R. Bensalem, J.J. Suñol, J. Alloys Compd. 494 (2010) 109–115.
[6] Z. Hua, W.Q. Yu, Y.M. Sun, S.H. Zhao, J. Alloys Compd. 505 (2010) 768–771.
[7] M. Pilar, L. Escoda, J.J. Suñol, J.M. Greneche, J. Magn. Magn. Mater. 320 (2008) e823–e827.
[8] Y.J. Liu, I.T.H. Chang, Mater. Sci. Eng. A 325 (2002) 25–30.
[9] B. Movahedi, M.H. Enayati, C.C. Wong, Mater. Lett. 64 (2010) 1055–1058.
[10] A. Inoue, Acta Mater. 48 (2000) 279–306.
[11] B. Majumdar, D. Akhtar, Mater. Sci. Technol. 21 (2005) 1139–1144.
[12] A.L. Greer, Nature 336 (1993) 303–304.
[13] D.Y. Liu, H.F. Zhang, Z.Q. Hu, W. Gao, J. Alloys Compd. 422 (2006) 28–31.
[14] M. Shapaan, J. Gubicza, J. Lendvai, L.K. Varga, Mater. Sci. Eng. A 375–377 (2004) 785–788.
[15] Y.J. Liu, I.T.H. Chang, P. Bowen, Mater. Sci. Eng. A 304–306 (2001) 389–393.
[16] A. Takeuchi, A. Inoue, Mater. Trans. 46 (2005) 2817–2829.
[17] A. Inoue, A. Takeuchi, T. Zhang, Metall. Mater. Trans. 29A (1998) 1779–1793.
[18] H.E. Kissinger, Anal. Chem. 29 (1957) 1702–1706.